




The Mini-SiTian Array: Optical Design

Zi-Jian Han^{1,2} , Zheng-Yang Li^{1,2}, Chao Chen^{1,2,3}, Jia-Nan Cong^{1,2,3}, Ting-Ting Liu^{1,2}, Yi-Ming Zhang^{1,2,3}, Qing-Shan Li⁴,
Liang Chen^{1,2}, and Wei-Bin Kong^{1,2}

¹ Nanjing Institute of Astronomical Optics & Technology, Chinese Academy of Sciences, Nanjing 210042, China; zyli@niaot.ac.cn

² CAS Key Laboratory of Astronomical Optics & Technology, Nanjing Institute of Astronomical Optics & Technology, Nanjing 210042, China

³ University of Chinese Academy of Sciences, Beijing 100049, China

⁴ Astronomical Engineering Co. Ltd., Tianjin 300380, China

Received 2024 December 16; revised 2025 February 19; accepted 2025 February 28; published 2025 May 6

Abstract

Time-domain astronomy is one of the most important areas. Large sky area, deep-field, and short timescale are the priority of time-domain observations. SiTian is an ambitious ground-based project processing all sky optical monitoring, aiming for a sky-survey timescale of less than 1 day. It is developed by the Chinese Academy of Sciences, an integrated network of dozens of 1 m class telescopes deployed worldwide. The Mini-SiTian Telescope Array is being carried out for demonstrations on optical design, group scheduling, and software pipeline developments, to overcome the high technical and financial difficulties of the SiTian project. One array contains three 300 mm F/3 telescopes, with an FOV of 5° over the 400–1000 nm wavelength range. The Mini-SiTian Telescope Array is now under commissioning in Xinglong Observatory, and a perfect platform for technical research and educational purposes.

Key words: telescopes – techniques: photometric – methods: observational

1. Introduction

Time-domain astronomy is one of the most important frontier areas. It aims to reveal the changes of various astronomical objects in the universe, as well as discover new astronomical objects and new phenomena through time-domain observations, including gravitational wave electromagnetic counterparts, exoplanet detection, and other popular directions in recent years. A series of influential large-scale time-domain survey projects such as the Panoramic Survey Telescope & Rapid Response System (Pan-STARRS, Kaiser et al. 2002), the Zwicky Transient Facility (ZTF, Bellm et al. 2019), and the Legacy Survey of Space and Time (LSST, Ivezić et al. 2019), are being carried out and planned to be implemented. Other ground-based sky-survey telescopes in China, such as the 2.5 m Wide-Field Survey Telescope (WFST, Lou et al. 2016) and the Multi-Channel Photometric Survey Telescope (Mephisto, Yuan et al. 2020) also have been under commissioning in the past two years, but they are all facing the shortcomings of observing many astronomical objects and phenomena effectively with changing timescales within one day cadence. The cadence of LSST, ZTF, and WFST is about 2–4 days, and the cadence of Mephisto is about 2 weeks. Only one telescope will not satisfy all the needs of large sky area, deep field, and high cadence simultaneously for time-domain sky survey observations. High-precision measurements enable the precise extraction of useful information from photometric variability, especially in scenarios where the amplitude of variability is relatively weak

(Li et al. 2022). Consequently, high-precision photometric survey telescopes are of great significance for research in the field of time-domain astronomy, such as the study of supernovae, AGNs, GRBs, and TDEs (Feng et al. 2021, Sun et al. 2024). The SiTian project is a next-generation, large-scale time-domain survey designed to build an array of 60 optical telescopes, primarily located at observatory sites in China. This array will enable single-exposure observations of the entire northern sky with a cadence of only 30 minutes, capturing true color (*gri*) time-series data down to about 21 mag. This project is proposed and led by the National Astronomical Observatories, Chinese Academy of Sciences (NAOC; Liu et al. 2021). The main science goals are the detection, identification, and monitoring of optical transients (such as gravitational wave event counterparts, fast radio bursts, and supernovae) on largely unknown timescales of less than 1 day. One SiTian node contains three prototype telescopes as an array (Chen et al. 2022), which have high technical difficulty and high financial requirements in early development, so it is relatively difficult to carry out key software technology breakthroughs such as telescope control and group scheduling in a short time. As the pathfinder for the SiTian project, the Mini-SiTian project (Huang et al. 2025) utilizes an array of three 300 mm telescopes to simulate a single node of the full SiTian array. The Mini-SiTian has begun its survey since 2022 November. One Mini-SiTian Array is composed of three 300 mm F/3 telescopes, with a field of view (FOV) of 5°, and can observe in *g*, *r*, and *i* bands. The tracking accuracy is root mean square

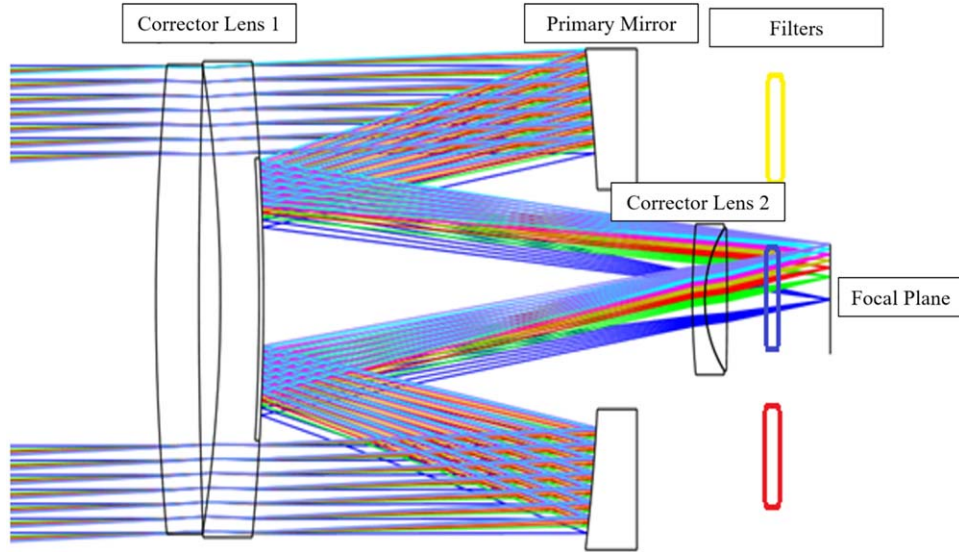


Figure 1. Optical layout of a Mini-SiTian Telescope.

(RMS) $\leq 0.5''$ in 10-minute observations of stars, and RMS $\leq 2.0''$ in observations of space targets.

In this article, the Mini-SiTian Telescope will be introduced. Instrument design will be described in Section 2, instrument performances in laboratory tests and commissioning will be showcased in Section 3, and the project will be summarized in Section 4.

2. Instrument

A Mini-SiTian Telescope is specifically designed for sky survey observations. With a large FOV and a fast focal ratio of F/3, the telescope uses a Cassegrain focus, on which the detector is easier to mount. The telescope has a good image quality on full FOV, which is capable of astrophotography, astronomical sky-survey, and space debris observations.

2.1. Optical Design

The optical system of a Mini-SiTian Telescope is based on heritage from the optical system of Chinese Small Telescope ARray (CSTAR, Liu & Yuan 2009). Evolved from the catadioptric optical system, it is a large FOV optical system that corrects the spherical aberration of the primary mirror at the entrance pupil to obtain a uniform star point spread function (PSF) distribution in the FOV. The telescope tube is compact with loose optomechanical tolerances. The disadvantage is that it is not easy to set up a stray light shield, leading to poor control of stray light, and thus requiring the addition of a front stray light shield. Key parameters of the telescope are listed in Table 1.

The optical layout is illustrated in Figure 1. The corrector lens belonging to group 1 serves as the incoming block window

Table 1
Key Parameters of a Mini-SiTian Telescope

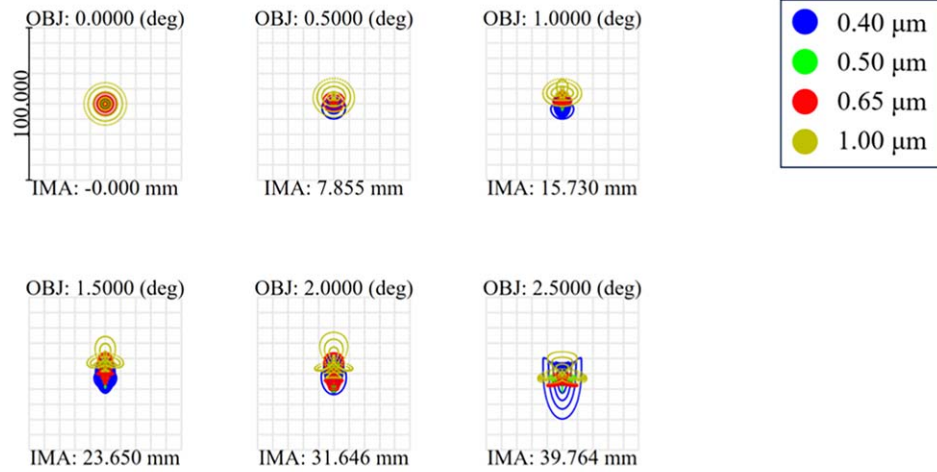
Parameter	Value
Aperture	300 mm
Focal length	900 mm
Focal ratio	F/3
Field of view	5°
Diameter of telescope tube	420 mm
Designed wavelength range	400–1000 nm
Weight	98 kg

of the telescope. Reflective coatings are made on the last surface to shorten the telescope tube. The corrector lens belonging to group 2 is used to enhance the image quality on marginal FOV. Three optical filters can be switched using a filter wheel. The size of the focal plane is Φ 80 mm, matching the FOV that is 5° in diameter.

The optical spot diagram and the diffraction encircled energy diagram are shown in Figures 2 and 3 respectively. The RMS radius is $8.728 \mu\text{m}$ at the maximum FOV of 5° over the wavelength range 400–1000 nm. The diameter of 80% encircled energy (EE80) is less than $5.04''$ ($\sim 10.94 \mu\text{m}$). Full width at half maximum (FWHM) is less than $2.89''$ ($\sim 6.29 \mu\text{m}$).

The telescope employs focusing mechanisms to compensate for defocus caused by transportation, temperature shifts, and optical path differences while switching wave band filters. Different wave band filters, *g*, *r*, and *i*, can be inserted into the optical path for multi-band observations.

Error budget analysis is essential in optical design to evaluate tolerances in manufacturing and mounting. Monte-



Surface: IMA						
Spot Diagram						
Lens has no title.						
Units are μm . Legend items refer to Wavelengths						
Field :	1	2	3	4	5	6
RMS radius :	4.554	4.740	5.850	7.734	8.276	8.399
GEO radius :	13.937	16.801	16.577	24.307	27.119	29.513
Scale bar :	100.000	Reference : Centroid				
						Configuration 1 of 1

Figure 2. Spot diagram of a Mini-SiTian Telescope.

Carlo analysis is performed on different FOVs to analyze the EE80 under different tolerances with ZEMAX software, which is shown in Figure 4. The results indicated that, at the central field with a 90% probability, the EE80 diameter is approximately $7.16 \mu\text{m}$ ($3''.31$). Furthermore, the EE80 diameter of the Mini-SiTian, under a 90% probability, was smaller than $8.21 \mu\text{m}$ ($3''.79$) for the maximum FOV, and the EE80 diameter of Mini-SiTian, under a 99% probability, was approximately $9.08 \mu\text{m}$ ($4''.19$) for the maximum FOV. These two values are extremely close, and this analysis confirmed that both the manufacturing process and the alignment are feasible.

As for the primary and secondary mirrors, enhanced aluminum coating is implemented. The average reflectance of the enhanced aluminum coating is 89.6% over 400–1000 nm. Anti-reflectance coatings are applied on the corrector lens, with an average transmittance of 97.4% over 400–1000 nm. By calculating all the working surfaces of the telescope optics, the overall efficiency of the telescope is about 68.5% over a range of 400–1000 nm, with minimum and maximum values of 64% and 74%, respectively.

2.2. Stray Light Analysis

Stray light refers to the light rays in an optical system that diffuse to the detector or imaging surface other than the target light rays and imaging light rays, as well as the target light rays

that reach the detector through abnormal optical paths. Stray light degrades the contrast and modulation transfer function (MTF) of the image plane, resulting in reduced image layers, deteriorated clarity, and disordered energy distribution. Furthermore, stray light can generate light spots on the image plane, or even completely overwhelm the target signal with stray radiation noise. Therefore, it is necessary to suppress stray light of a Mini-SiTian Telescope.

The suppression level of stray light in optical-mechanical systems is generally evaluated using Point Source Transmittance (PST). PST is defined as the ratio of the irradiance reaching the detector surface after the radiation from a point source target at an off-axis angle of θ at wavelength λ outside the system's FOV passes through the optical-mechanical system $E_{\text{image}}(\theta, \lambda)$, to the irradiance of that light source at the system's entrance aperture $E_{\text{ea}}(\theta, \lambda)$, which is

$$\text{PST} = \frac{E_{\text{image}}(\theta, \lambda)}{E_{\text{ea}}(\theta, \lambda)}. \quad (1)$$

Due to the compact structure and large FOV of the telescope, it is difficult to place a large baffle inside the telescope to suppress stray light. Especially when the incident angle of stray light is small, the telescope image is severely affected by stray light, leading to obvious ghost images. To more effectively suppress stray light, a long baffle needs to be installed in front of the telescope. Figure 5(a) and (b) shows the stray light

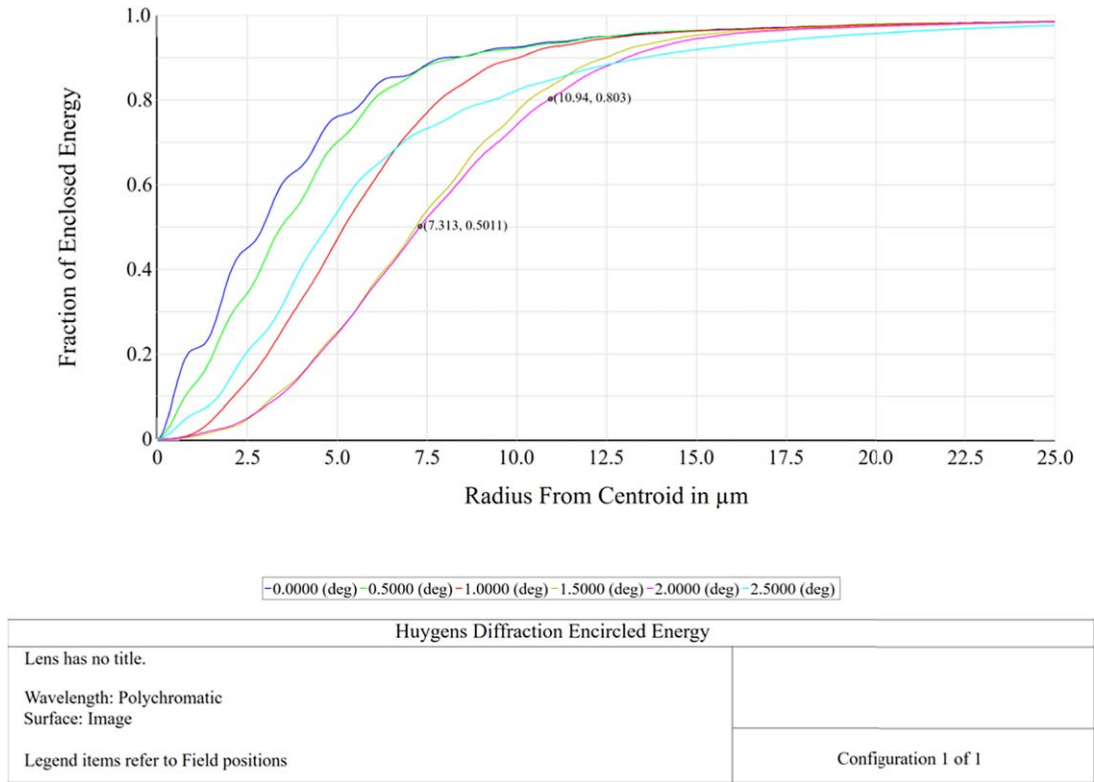


Figure 3. Diffraction encircled energy of a Mini-SiTian Telescope.

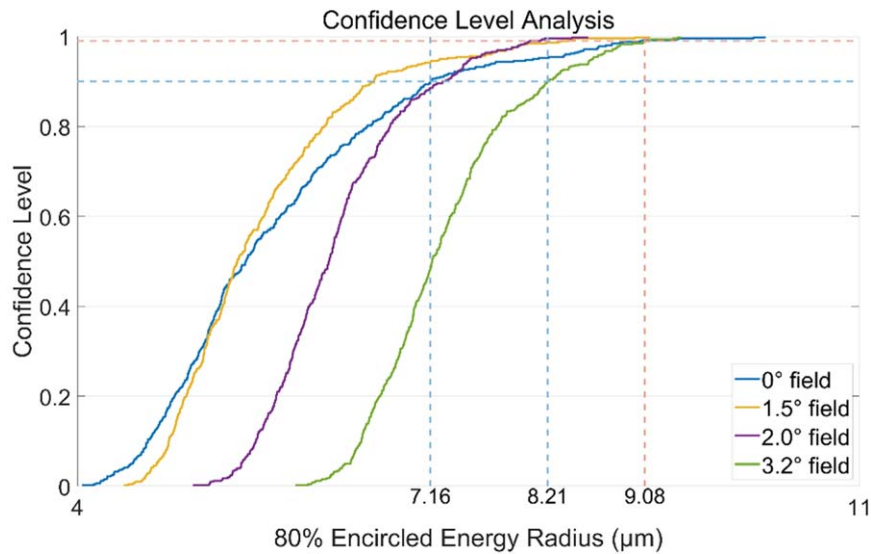


Figure 4. Results of the error budget analysis.

analysis optical-mechanical models without and with the front baffle, respectively.

Figure 6(a) and (b) present the illuminance of stray light on the image plane at a 15° incident angle without and with the

front baffle, respectively, where the irradiance of the stray light source is 1 W m^{-2} . When no front baffle is used, the stray light brightness on the image plane is high, and a bright ghost image appears on the left side of the image plane. By using the front

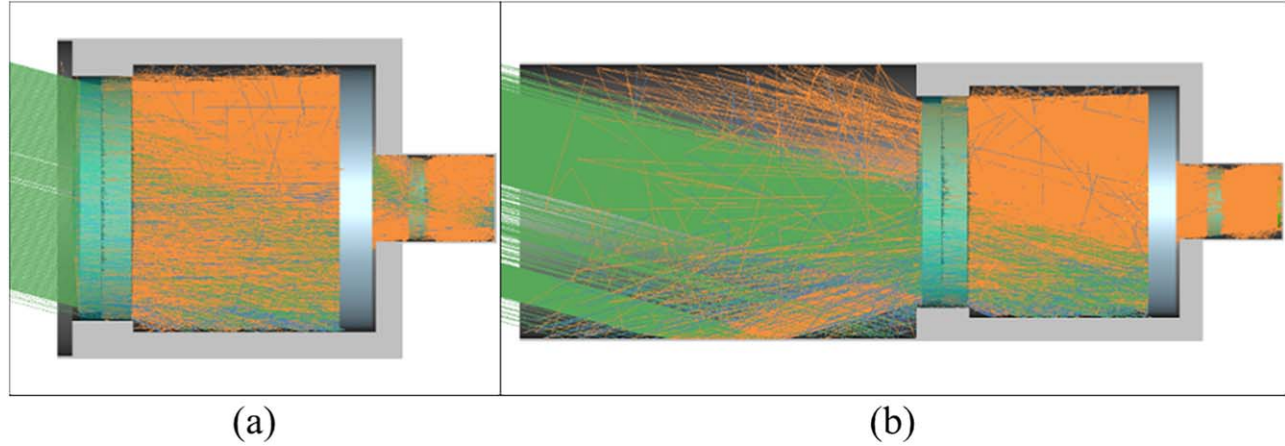


Figure 5. Stray light suppression (a) with and (b) without a front baffle of 60 cm in length.

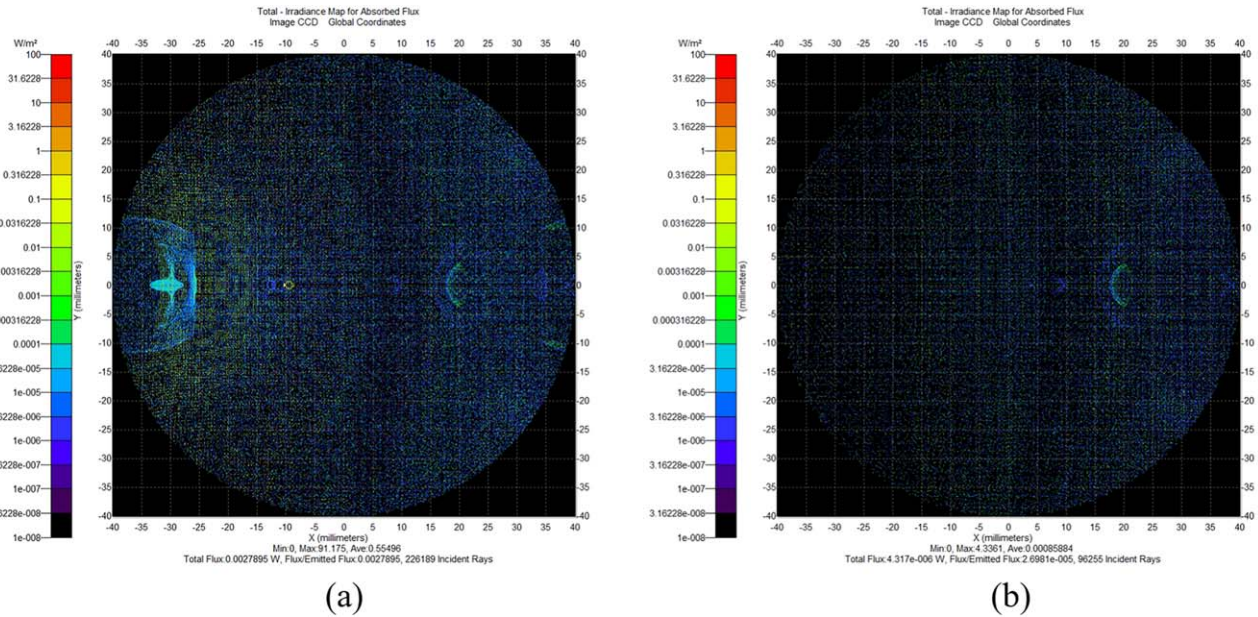


Figure 6. Distribution of stray light on the image plane (a) without a front baffle and (b) with a 60 cm front baffle, both under an irradiance of 1 W m^{-2} for the stray light source.

baffle, the stray light brightness and ghost image on the image plane are effectively suppressed.

Figure 7 shows the PST curves for both cases. Without the baffle, the incident angle of stray light needs to be above 30° for the system’s PST to decrease to the order of 10^{-4} ; with the front baffle, this requirement is reduced to 15° .

2.3. Equatorial Mount

The equatorial mount is specially designed for sky-survey observations, as shown in Figure 8. It uses Computerized Numerical Control (CNC) integrated processing and forming in

manufacturing. To guarantee pointing and tracking accuracy, the equatorial mount uses an axial magnetic field torque motor and a high-precision industrial-grade 32-bit absolute encoder. The pointing accuracy is better than $10''$ after pointing modeling, and the star-tracking accuracy is better than $0.5''$ over 10 minutes. The equatorial mount can also be used for space target observations, with tracking accuracy better than $2''$.

The equatorial mount can be operated on either a Windows or Linux platform, and it can also be operated with a SkyView graphical user interface (GUI). It supports ASCOM RTS2 protocols, and third-party software such as SkyX. SDK and

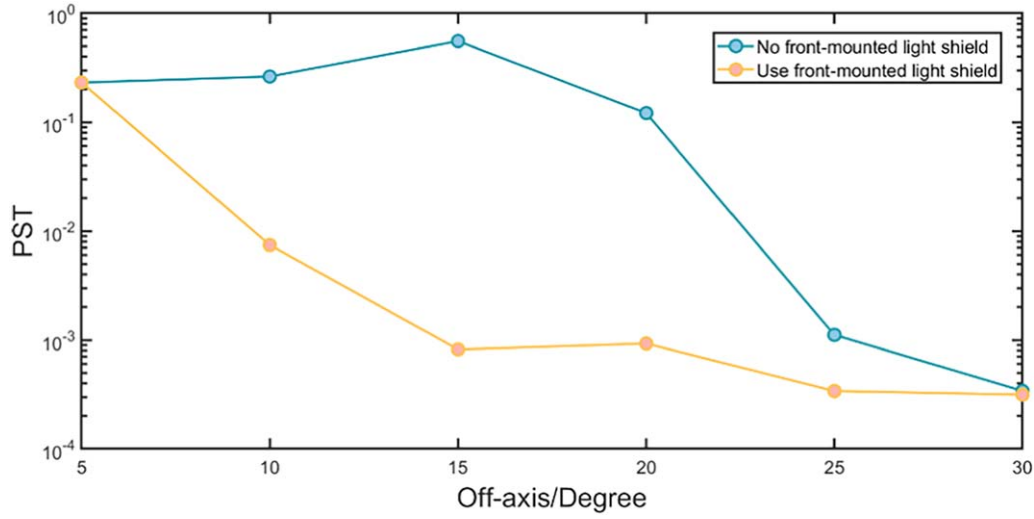


Figure 7. PST curves for the cases with and without a front baffle.

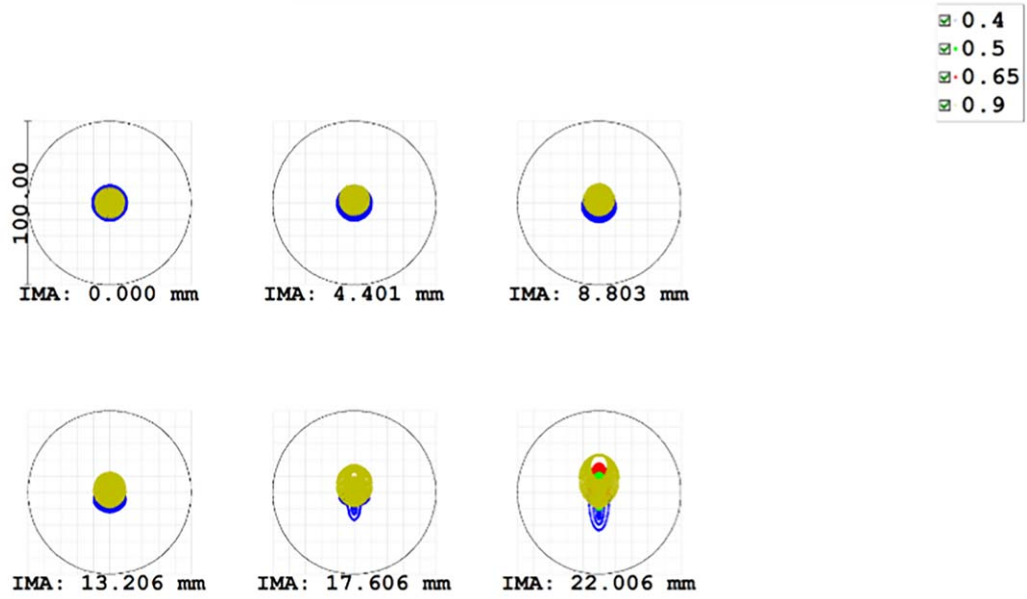


Figure 8. Equatorial mount of a Mini-SiTian Telescope Array in the factory.

low-level commands are provided for further development purposes.

As shown in Figure 8, the equatorial mount can be quickly switched between alt-azimuth and equatorial

configurations, without any lifting equipment. The telescope mount has a maximum loading capacity of 200 kg. The maximum power of the mount is 800W with a 200 240 VAC power supply.



Surface: IMA

Spot Diagram							NIAOT zyli@niaot.ac.cn	
Lens has no title., 2021/7/20								
Units are μm . Legend items refer to Wavelengths								
Field :	1	2	3	4	5	6		
RMS radius :	5.708	5.704	5.532	5.824	6.259	8.956		
GEO radius :	10.552	10.898	11.408	12.217	16.694	23.087		
Circle diam:	100	Reference	: Middle					

Figure 9. Tested spot diagram of a Mini-SiTian Telescope.

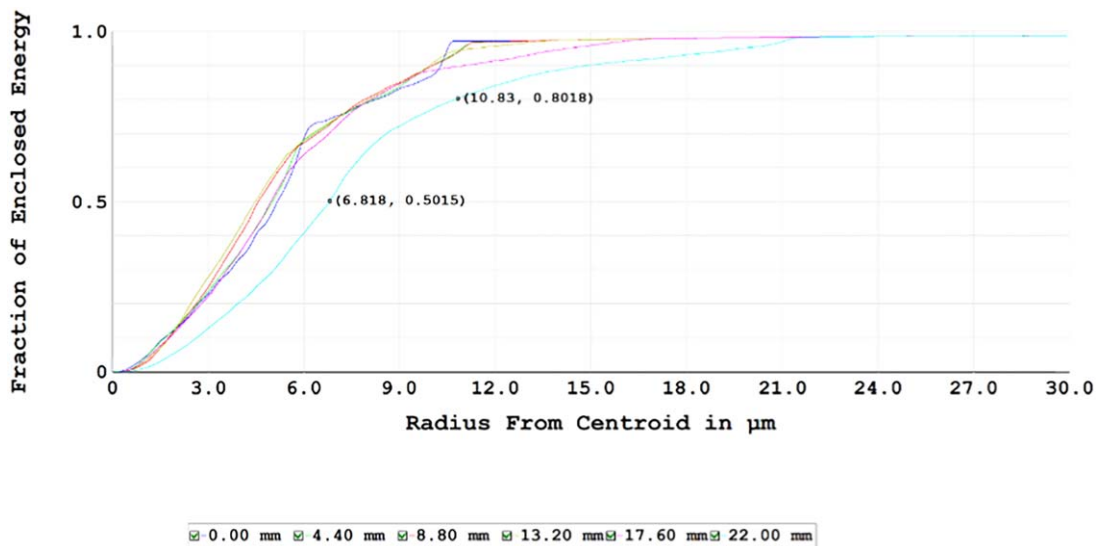


Figure 10. Tested diffraction encircled energy of a Mini-SiTian Telescope.

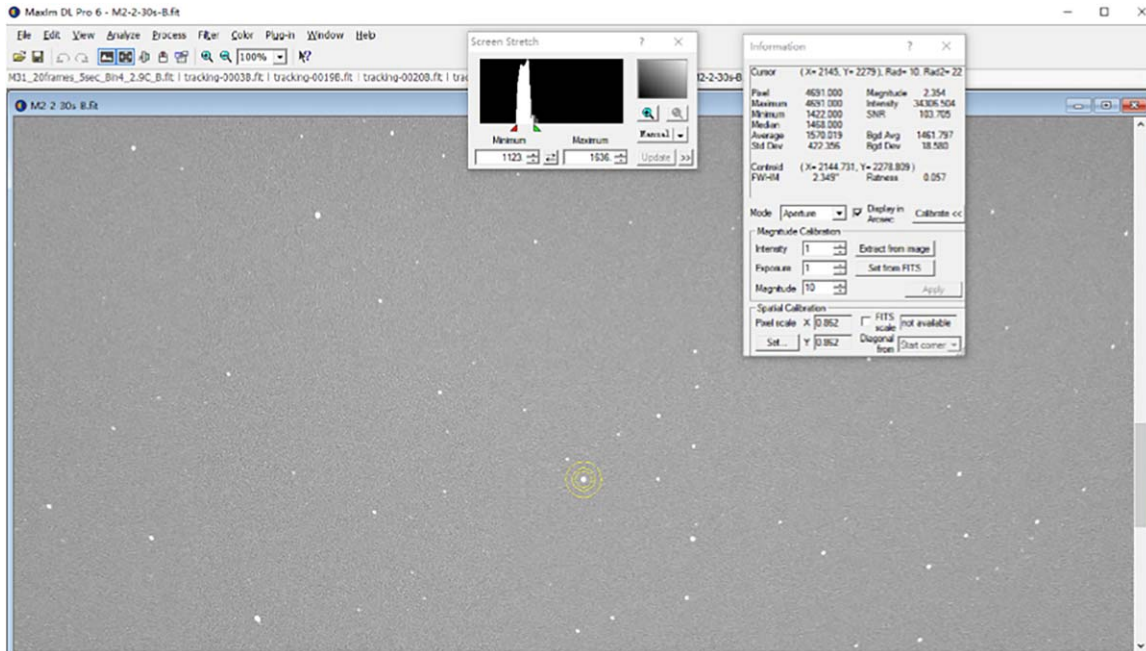


Figure 11. The tested minimum FWHM of the image is $2''.35$.

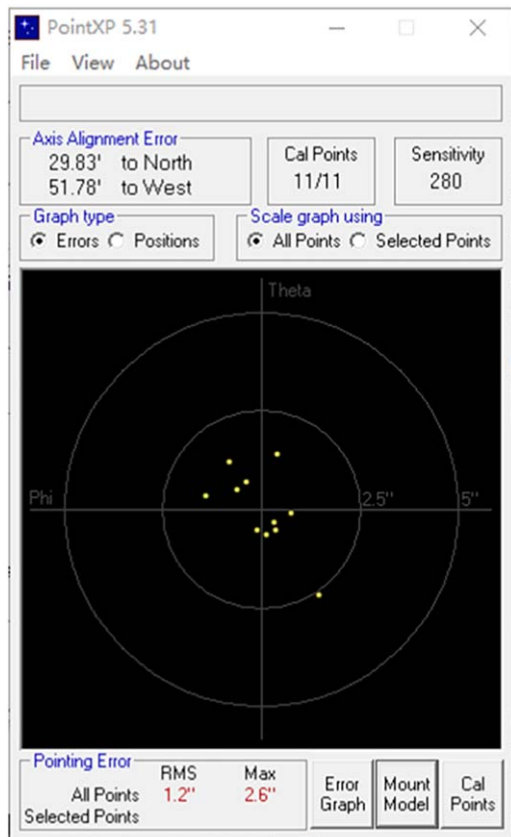


Figure 12. The tested RMS of pointing error is $1''.2$.

3. Performance

3.1. Testing Observations

Image quality, pointing accuracy, and tracking ability were tested in Nanjing, China, in 2021 July. With manufacturing error incorporated into the optical design, the EE80 diameter of the optical system is about $5''.1$, and the FWHM is less than $3''.4$. The tested spot diagram and tested diffraction encircled energy diagram are shown in Figures 9 and 10, respectively.

To evaluate the imaging performance, the telescope features a ZWO ASI6200MM Pro CMOS camera mounted on its back. The size of the camera sensor is $36\text{ mm} \times 24\text{ mm}$, corresponding to an FOV of 2.3×1.53 . The tested minimum FWHM is $2''.35$, as Figure 11 affirms.

3.2. Pointing and Tracking Abilities

Pointing modeling is done before testing observations. The maximum pointing error is $2''.6$, and the RMS value is $1''.2$, as Figure 12 shows. The pointing error is much lower than the requirement ($<10''$).

To test the tracking ability, a star is observed by the telescope without any guide stars. Figure 13 shows the tracking ability when observing a star over 10 minutes. RA RMS is $0''.175$ and DEC RMS is $0''.03$. The tracking accuracy of both axes is lower than the design requirements ($0''.5$). A satellite is also observed to test the tracking accuracy. As Figure 14 shows, RA RMS is $1''.297$, and DEC RMS is $0''.660$. The result

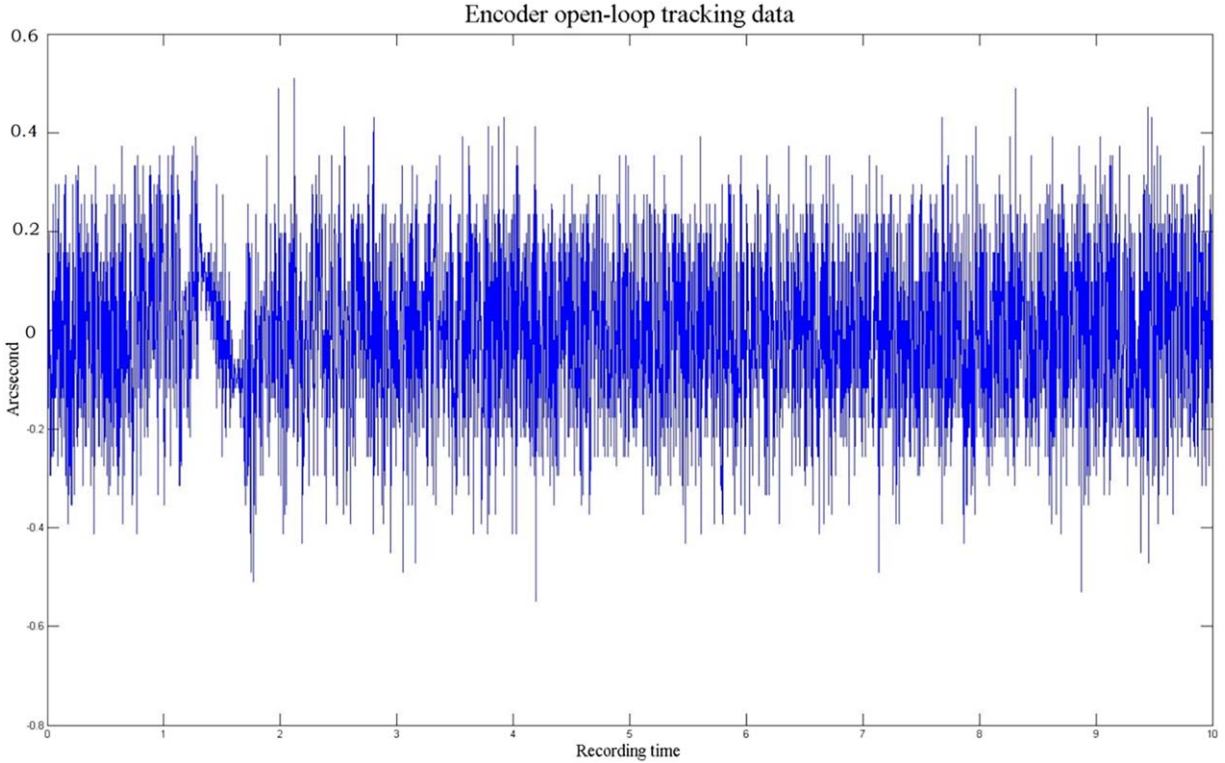


Figure 13. Tracking accuracy of a Mini-SiTian Telescope when observing a star.

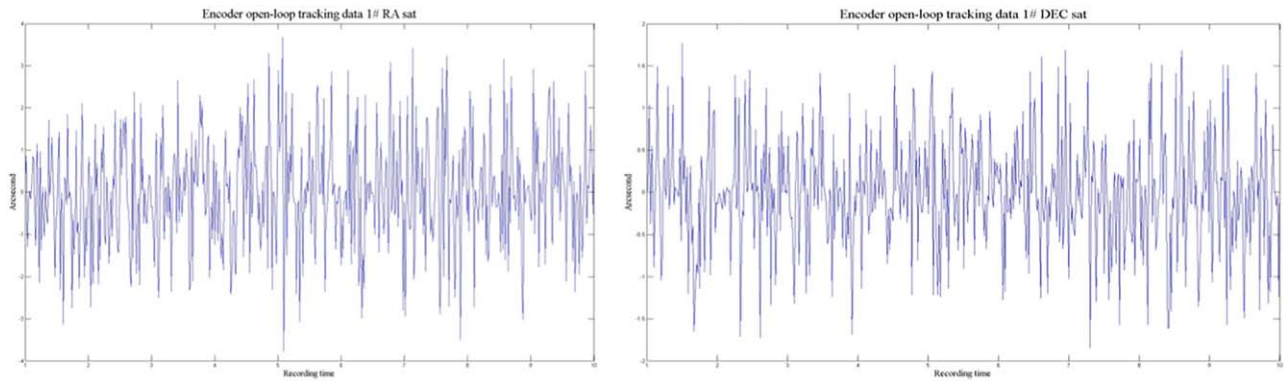


Figure 14. Tracking accuracy of a Mini-SiTian Telescope when observing a satellite.

shows the perfect tracking ability of the Mini-SiTian Telescope Array.

3.3. Commissioning

The Mini-SiTian Telescope Array was transported to Xinglong Observatory of NAOC, in 2021 August. The Xinglong Observatory is located at $40^{\circ}23'39''\text{N}$, $117^{\circ}34'30''\text{E}$, with ~ 900 m average altitude. The mean and median seeing values of the Xinglong Observatory are $1.9''$ and $1.7''$,

respectively. Most of the time, the sky brightness is about $21.1 \text{ mag arcsec}^{-2}$ in V band at the zenith. The mounted Mini-SiTian Telescope Array at Xinglong Observatory is depicted in Figure 15.

4. Conclusions

The Mini-SiTian Telescope Array is a demonstration platform for the SiTian project. Three telescopes are combined in one node to realize multi-color observations. The 300 mm F/

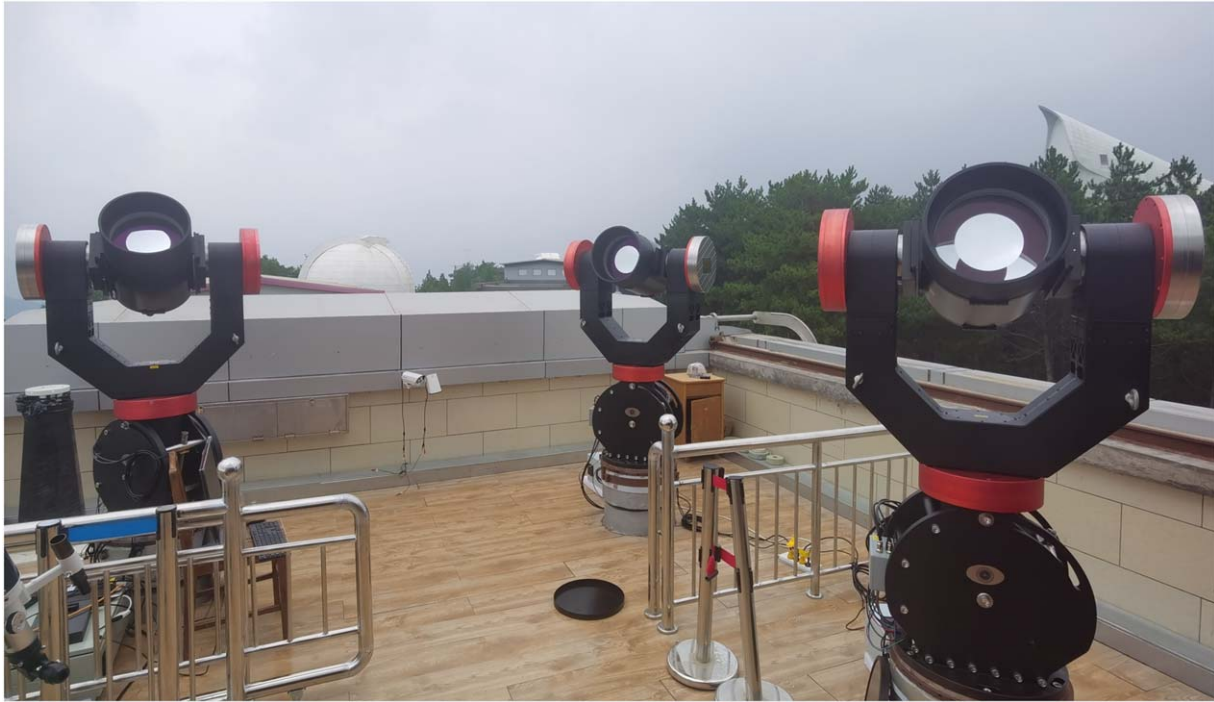


Figure 15. The Mini-SiTian Telescope Array commissioning at Xinglong Observatory.

3 telescope has an FOV of 5° , which is specially designed for sky survey imaging. Commissioning in Xinglong Observatory, and developing the software pipeline and control strategy have been successfully demonstrated and verified. The Mini-SiTian Telescope Array has proved to be a perfect platform for technical research and educational purposes.

Acknowledgments

The SiTian project is a next-generation, large-scale time-domain survey designed to build an array of over 60 optical telescopes, primarily located at observatory sites in China. This array will enable single-exposure observations of the entire northern hemisphere night sky with a cadence of only 30 minutes, capturing true color (*gri*) time-series data down to about 21 mag. This project is proposed and led by the National Astronomical Observatories, Chinese Academy of Sciences (NAOC). As the pathfinder for the SiTian project, the Mini-SiTian project utilizes an array of three 30 cm telescopes to simulate a single node of the full SiTian array. The Mini-SiTian began its survey in 2022 November. The SiTian and Mini-SiTian have been supported from the Strategic Pioneer

Program of the Astronomy Large-Scale Scientific Facility, Chinese Academy of Sciences and the Science and Education Integration Funding of University of Chinese Academy of Sciences. This work is supported by the National Key Basic R&D Program of China via 2023YFA1608304.

ORCID iDs

Zi-Jian Han  <https://orcid.org/0000-0002-4614-1365>

References

- Bellm, E. C., Kulkarni, S. R., Graham, M. J., et al. 2019, *PASP*, **131**, 018002
 Chen, C., Li, Z., Liu, J., Han, Z., & Yuan, X. 2022, *Proc. SPIE*, **12315**, 1231504
 Feng, H.-C., Hu, C., Li, S.-S., et al. 2021, *ApJ*, **909**, 18
 Huang, Y., Liu, J.-F., Wu, H., et al. 2025, *RAA*, **25**, 044001
 Ivezić, Ž., Kahn, S. M., Tyson, J. A., et al. 2019, *ApJ*, **873**, 111
 Kaiser, N., Aussel, H., Burke, B. E., et al. 2002, *Proc. SPIE*, **4836**, 154
 Li, S.-S., Feng, H.-C., Liu, H. T., et al. 2022, *ApJ*, **936**, 75
 Liu, G. R., & Yuan, X. Y. 2009, *AcASn*, **50**, 224
 Liu, J., Soria, R., Wu, X.-F., et al. 2021, *AnABC*, **93**, 20200628
 Lou, Z., Liang, M., Yao, D., et al. 2016, *Proc. SPIE*, **10154**, 101542A
 Sun, T.-R., Geng, J.-J., Yan, J.-Z., et al. 2024, *ApJL*, **976**, L20
 Yuan, X., Li, Z., Liu, X., et al. 2020, *Proc. SPIE*, **11445**, 114457M